Natural strong pinning sites in laser-ablated $YBa_2Cu_3O_{7-\delta}$ thin films

J. M. Huijbregtse, B. Dam,* R. C. F. van der Geest, F. C. Klaassen, R. Elberse, J. H. Rector, and R. Griessen
Faculty of Sciences, Division of Physics and Astronomy, Vrije Universiteit, De Boelelaan 1081, NL-1081 HV Amsterdam, The Netherlands

(Received 19 January 2000)

At low temperatures dislocations are the dominant flux-pinning centers in thin films of $YBa_2Cu_3O_{7-\delta}$ deposited on (100) $SrTiO_3$ substrates [B. Dam *et al.*, Nature (London) **399**, 439 (1999)]. Using a wet-chemical etching technique in combination with atomic force microscopy, both the length and the lateral dislocation distribution are determined in laser ablated $YBa_2Cu_3O_{7-\delta}$ films. We find that (i) dislocations are induced in the first stages of film growth, i.e., close to the substrate-film interface, and persist all the way up to the film surface parallel to the *c* axis, resulting in a uniform length distribution, and (ii) the radial dislocation distribution function exhibits a universal behavior: it approaches zero at small distances, indicating short-range ordering of the defects. This self-organization of the growth-induced correlated disorder makes epitaxial films completely different from single crystals with randomly distributed columnar defects created by means of heavy-ion irradiation. Since the substrate temperature can be used to tune the dislocation density $n_{\rm disl}$ over almost two orders of magnitude (~ 1–$100/\mu m^2$), the mechanism by which dislocations are induced is closely related to the $YBa_2Cu_3O_{7-\delta}$ nucleation and growth mechanism. We present evidence for preferential precipitation in the first monolayer and precipitate generated dislocations.

I. INTRODUCTION

In the last few years the quality of high-T_c superconducting thin films has improved significantly. Thin films have become more and more single-crystalline like. However, the magnitude of the critical current density j_c in films is still orders of magnitude higher than in single crystals. In $YBa_2Cu_3O_{7-\delta}$ films, for example, j_c is as high as 10^{12} A/m^2 (at small magnetic fields and low temperatures) while in single crystals it is typically 10^{10} A/m^2.[1] The high j_c of films is generally attributed[2] to the strong pinning[3,4] of vortices to extended defects. In single crystals the transport properties are mainly determined by randomly distributed point defects (e.g., oxygen vacancies), leading to weak collective pinning.[4] The high j_c values found in films must thus be caused by extended defects which are specific for films such as substrate induced antiphase boundaries,[5] dislocations,[6–8] or surface roughness.[8,9] Although there are experimental results[10,11] pointing to the importance of pinning by *dislocations* in films, until recently no quantitative relation between the dislocation density and the pinning properties could be established.

By comparing $YBa_2Cu_3O_{7-\delta}$ films with widely differing dislocation densities $n_{\rm disl}$ we observed[12] a universal magnetic-field dependence of the critical current density (see Fig. 1): j_c is constant up to a certain characteristic field B^* and decays rapidly according to a power law $j_c \propto 1/B^\alpha$ above this field[13] (with $0.5<\alpha<1.0$). The characteristic field B^* is proportional to $n_{\rm disl}$ with a proportionality constant of $0.7\Phi_0$ per dislocation (where Φ_0 is the flux quantum), indicating that dislocations are responsible for the high critical currents in $YBa_2Cu_3O_{7-\delta}$ films. The magnitude of j_c for $B<B^*$, however, does *not* depend strongly on the defect density.[12] For all films we find j_c values in the range 10^{11}–10^{12} A/m^2 (at 4.2 K). In other words, j_c below B^* is solely determined by vortices that are individually pinned along dislocations.

Interestingly, dislocations are induced by the thin-film growth process itself. In the present paper, we investigate the dislocation structure in laser-ablated $YBa_2Cu_3O_{7-\delta}$ films and its origin in detail. Instead of looking at the as-grown surface morphology, we investigate wet-etched films. It has been suggested[6] that the density of *screw* dislocations can be determined by counting the number of spiral outcrops[14,15] at the film surface. However, in this way the total dislocation density (edge, screw, and dislocations of mixed character) is severely underestimated[16] for two reasons: (i) edge dislocations do not give rise to any topological structure and (ii) not

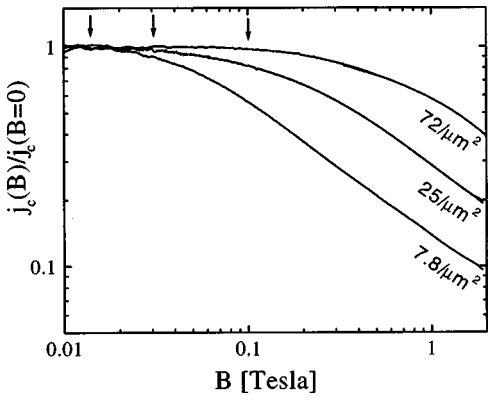

FIG. 1. Critical current density j_c at 10 K as a function of the magnetic field B for three $YBa_2Cu_3O_{7-\delta}$ films laser deposited on (100) $SrTiO_3$ with dislocation densities $n_{\rm disl}=7.8$, 25, and $72/\mu m^2$. $j_c(B)$ is measured by means of torque magnetometry (using a sweep rate of 1 mT/s) and normalized to $j_c(B=0)=6.6\times10^{11}$, 4.1×10^{11}, and 3.7×10^{11} A/m^2, respectively. The critical current is constant up to a characteristic field B^*, as indicated by arrows, and decays rapidly at higher fields. B^* increases linearly with $n_{\rm disl}$ with a proportionality constant of $0.7\Phi_0$.

all screw dislocations generate growth spirals. Wet-chemical etching in combination with atomic force microscopy reveals the full dislocation structure and allows for a statistical analysis. Not only the length but also the lateral dislocation distribution can be determined. In this way important information about the pinning energy landscape in $YBa_2Cu_3O_{7-\delta}$ films is obtained. Moreover, it appears that in films grown on (100) MgO substrates even high-angle grain boundaries are resolved. Therefore wet-chemical etching is also an attractive tool for studying weak links in $YBa_2Cu_3O_{7-\delta}$ films.

We find that dislocations are generated in the early stages of growth, i.e., close to the substrate-film interface. Since dislocations cannot end inside a crystal,[17] they persist up to the film surface parallel to the *c* axis, resulting in a uniform length distribution. Consequently, they can pin vortices along their entire length. At first sight this situation seems very similar to *artificial* linear defects created by irradiating single crystals with heavy ions.[18,19] However, in our films the linear defects are *growth induced* and also exhibit short-range ordering, whereas artificial columnar defects are randomly distributed. The nonrandom dislocation distribution enhances the pinning efficiency even more. Since we can also tune the dislocation density at will without affecting either the length or the lateral distribution of these linear defects, we now have a very attractive system to study vortex matter. For instance, the predicted Mott-insulator vortex phase[3,20] may be observable in thick laser-ablated $YBa_2Cu_3O_{7-\delta}$ films at low dislocation densities.

II. EXPERIMENTAL PROCEDURE

C-axis oriented $YBa_2Cu_3O_{7-\delta}$ films are deposited on (100) $SrTiO_3$ and (100) MgO substrates by means of pulsed laser deposition (PLD). The 30-ns, 248-nm excimer laser beam (QUESTEK Impulse 4750GL: fluence 1.3 J/cm^2, repetition rate 5 Hz) is guided into an UHV deposition system using projection optics[21] to ensure a reproducible deposition process.[22] The films are deposited from a polycrystalline, high-density, single phase, tetragonal $YBa_2Cu_3O_{6+x}$ target (PRAXAIR, 99.995% pure raw materials) using substrate temperatures T_{sub} between 750 and 850 °C, as measured with a pyrometer. The background oxygen pressure p_{O2} is varied from 15 up to 50 Pa using substrate-target distances $d_{T\text{-}S}$ between 3.0 and 3.5 cm. Our laser-ablated films generally follow a two-dimensional (2D) nucleation and growth mode.[16,23] The size *D* of the growth islands can be modified reproducibly between 125 and 450 nm by adjusting the deposition conditions: raising T_{sub} and/or p_{O2} (while keeping the substrate in the top of the plume by properly adjusting $d_{T\text{-}S}$) results in larger growth features.[23]

For comparison, also some $YBa_2Cu_3O_{7-\delta}$ films sputtered on (100) $SrTiO_3$ were investigated. Using dc sputtering at 840 °C and 3 mbar's oxygen pressure with a substrate-target distance of 2 cm,[24] films containing large growth spirals (>2 μm) are obtained. In contrast to PLD films, these sputtered films need to be post annealed for 1 h at 650 °C in 10^3 mbar's O_2 in order to optimize the superconducting properties.

The PLD and sputtered films have a thickness of typically 140 and 200 nm, respectively, except when mentioned otherwise. The superconducting and structural properties of all these films are excellent. For instance, the transition temperature of the PLD films[22] used in this investigation is 90 K or higher (with a transition width of less than 0.5 K), as determined from four-point electrical resistance measurements. X-ray-diffraction measurements indicate perfect *c*-axis orientation and a high degree of crystallinity (rocking curve widths of the 005 reflection $\Delta\omega_{005} \approx 0.1°$).

The aim of this work is to investigate the dislocation structure in these films as a function of the deposition conditions. As is well known in metallurgy,[25] dislocation densities can be determined by counting the number of etch pits formed upon applying a suitable dislocation sensitive etchand. In the case of $YBa_2Cu_3O_{7-\delta}$, we use a 1 vol % Br in ethanol solution.[16,26–29] To analyze the surface morphology of both the as-grown and the etched films, we use scanning tunneling microscopy (STM) and atomic force microscopy (AFM) in the tapping mode (NANOSCOPE IIIa multimode system). STM measurements are performed in the constant current mode using mechanically sharpened PtIr tips, operated at a bias voltage of 700 mV and tunneling currents around 100 pA.

In order to investigate the *persistence* of etch pits upon repeated etching, a specific area on the film surface is identified by means of two perpendicular engraved markers. Using the large range of the tube scanner (maximum scan size 100 μm), horizontal displacements of the AFM tip of about 20 μm with respect to these reference markers can be reproduced. In this way surface features can be traced back, even after repeatedly etching and remounting of the sample.

III. REVEALING DISLOCATIONS

In this section we show how wet-chemical etching in 1 vol % Br ethanol reveals dislocations. As a first step, the development of etch pits at defect sites is described. Since sputtered films exhibit spiral outcrops (i.e., screw dislocations), we use these film to test our etching technique. Finally the persistence of etch pits upon repeated etching at defect sites is probed in PLD films, indicating that the defects that are revealed are indeed *linear* defects.

A. Principle of etching

The surface morphology of as-grown PLD films is generally characterized by a semiregularly spaced array of growth islands, separated by trenches [see Fig. 2(a)]. These trenches have a depth up to 20% of the film thickness. In the trenches some deeper depressions can be discerned. Changing the deposition conditions (T_{sub} and p_{O2}) mainly affects the size *D* of the islands, i.e., the spacing between trenches. Since our PLD films grow by 2D nucleation and growth,[16,23] we find no spiral outcrops at the surface. Therefore from the surface morphology only, it is not possible to determine the (screw) dislocation density.

In order to reveal dislocations ending at the film surface, we apply a dislocation sensitive etchand. For etching to start on a flat, defect-free crystal surface, a negative 2D nucleus has to be formed.[25,30] Analogous to growth by 2D nucleation, the radius of this nucleus, *R*, has to exceed some critical value R^* to become a stable and expanding nucleus. This is due to the positive edge free-energy term in the total Gibb's free-energy change:

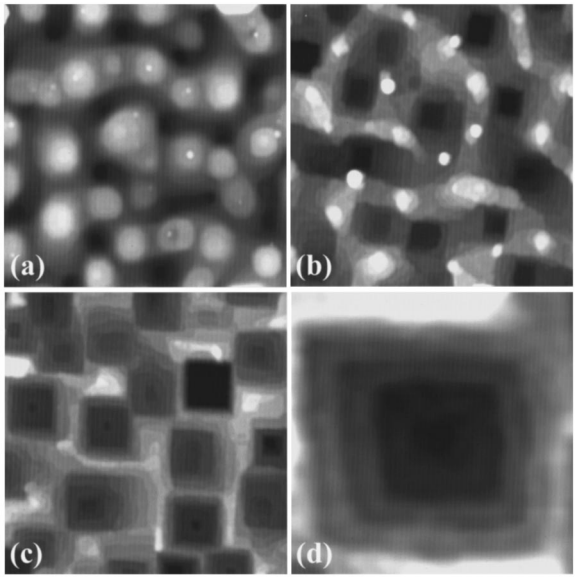

FIG. 2. Surface morphology of a 110-nm-thick $YBa_2Cu_3O_{7-\delta}$ film laser deposited on (100) $SrTiO_3$ and subsequently etched in 1 vol % Br ethanol: (a) as-grown surface morphology consisting of semiregularly spaced growth islands separated by trenches, (b) after 5 s of etching both the as-grown surface morphology and the formation of etch pits can be discerned, and (c) after 10 s of etching only sharp-bottomed etch pits are visible. In these three AFM height images of $1.0\times1.0\ \mu m^2$ dark is low and bright is high. In (d) a closeup ($225\times225\ nm^2$) of an etch pit is shown that consists of steps of several unit cells (u.c.) in height: 11 nm (5 u.c.), 2.4 (2 u.c.), 3.6 nm (3 u.c.), and 2.4 nm (2 u.c.) from high (bright) to low (dark), corresponding to an average inclination angle of 7.5°.

$$\Delta G(R) = -\pi R^2 h \Delta\mu + 2\pi R \gamma h. \quad (1)$$

Here γ is the edge free energy, h the height of the nucleus, and $\Delta\mu$ the difference in chemical potential between atoms in the solid and those dissolved ($\Delta\mu>0$). After a stable (negative) nucleus has been formed, dissolution proceeds by fast lateral movement of the negative steps. In the absence of defects, nucleation is a random process and the crystal gets thinner, while, on average, the surface remains flat.

The situation is different in the presence of defects. A defect provides for a site where locally either γ is reduced and/or $\Delta\mu$ is increased, i.e., a site where the activation energy for dissolution is lowered. Therefore at defect sites repetitive preferential nucleation takes place and an etch pit forms. However, as soon as the defect ends, there is no longer a source for preferential nucleation and the surface gets flat again. In the case of linear, i.e., extended defects, repetitive preferential nucleation at linear defect sites results in *persistent*, sharp-bottomed etch pits.

As follows from Fig. 2(a), as-grown PLD films are not flat. Upon etching a film with a rough surface, but without defects, steps proceed by fast lateral movement and the surface smoothens upon etching. In the presence of linear defects, the roughness first increases [creation of etch pits, whereas the original surface roughness has not yet been smoothed, see Fig. 2(b)] and then decreases [etch pits persist, whereas the surface in between the pits becomes flatter, see Fig. 2(c)]. Hence upon etching $YBa_2Cu_3O_{7-\delta}$ films in Br ethanol the growth islands are erased and an ensemble of square, sharp-bottomed etch pits forms. As shown in Fig. 2(d), within an etch pit concentric steps can be discerned. These steps are usually several unit cells in height. Clearly, the pits are not negative spirals. Negative spirals are only expected at extremely small undersaturations.[31] As the etch pits are symmetric,[32] we infer that the dislocation line is perpendicular to the film plane (i.e., parallel to the *c* axis). The square edges of the pits are roughly parallel to the [100] and [010] directions, indicating that the etch pit shape is determined by the slowest etching step directions. These directions are indeed parallel to the strongest chemical bonds.[33] Since on $SrTiO_3$ substrates all etch pits have the same orientation, we infer that the in-plane crystal orientation of the films is good (except for the occurrence of twin boundaries which are generally present in $YBa_2Cu_3O_{7-\delta}$ films deposited on $SrTiO_3$). The etch pits are not bounded by low index crystal planes. The slope of the sides of the etch pits varies between 7 and 12° and appears to be determined by the etching kinetics.

B. Etching sputtered films

To prove that we are revealing *dislocations*, we etched sputtered films. The surface morphology of sputtered films consists of large growth spirals of unit-cell step height and a large (>100 nm) step spacing, resulting in islands up to 2.5 μm in diameter.[12] Since sputtered films grow in a spiral growth mode, we can exactly identify the position where *screw* dislocations are located (i.e., at the spiral outcrop). We find that etch pits develop both at the spiral core and randomly around the core (see Fig. 1a in Ref. 12). The pit at the spiral core has to be due to a screw dislocation and from the unit-cell height we infer that this dislocation has a Burgers vector of 1.2 nm.

Generally, the vertical etch rate is determined by the stress field around the dislocation. Since the magnitude of the stress depends on the size of the Burger's vector and not on its direction, etching reveals all dislocations. Therefore the pits within the spiral that are not related to any growth feature have to be of an edge character.

We note that the spiral in Ref. 12 is in fact a double spiral originating from two screw dislocations with Burger's vectors of opposite sign.[34] Consequently, also at the other end of the spiral a screw dislocation is expected. Indeed,[12] we find another etch pit exactly at this position, proving that dislocations are revealed.

C. Repetitive etching

How do we prove that the defects, which are revealed by etching, are really *linear* defects, i.e., defects that have a length comparable to the film thickness? To answer this question we followed an ensemble of etch pits upon *repeated* etching PLD films, by marking an area on the film surface using a set of engraved perpendicular markers. Since both the depth of etch pits increases and the film thickness decreases upon repeated etching, we are able to follow the etch pits *in* the film. A sequence of consecutive etch experiments is shown in Fig. 3. In this figure, it can be seen that etch pits develop at the periphery of the islands and that all etch pits persist upon repeated etching. Since the bottoms of the etch pits do not turn flat but remain sharp, there is a persistent

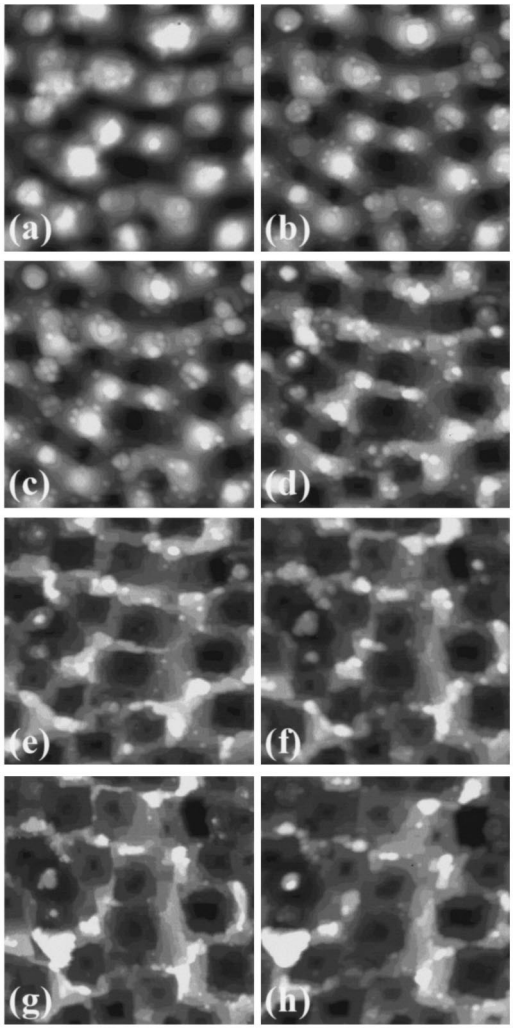

FIG. 3. Surface morphology of a 490-nm-thick $YBa_2Cu_3O_{7-\delta}$ film laser deposited on (100) $SrTiO_3$. Consecutive AFM height images are taken after repetitive etching of the same area ($0.5 \times 0.5\ \mu m^2$): (a) as deposited, (b) 10 s, (c) 15 s, (d) 20 s, (e) 25 s, (f) 30 s, (g) 35 s, and (h) 40 s etched, showing the persistence of etch pits upon prolonged etching. The average etching rate, estimated by fully etching off the film, is about 1 nm/s. In the upper left corner, a precipitate is revealed upon etching.

source for preferential etching. Thus we conclude that we are indeed dealing with linear defects of a considerable length.

In Fig. 3 some etch pits are hampered in their development (see, for instance, the etch pit in the upper left corner). Upon prolonged etching first a precipitate is revealed and then an etch pit forms again, indicating that dislocations can end and originate again at precipitates.[17] However, in all etching experiments this fraction is small ($<5\%$).

Since the lateral size of the etch pits increases upon repeated etching (Fig. 3), it becomes more and more difficult to follow the individual etch pits. Although initially overlapping etch pits can still be distinguished due to their pronounced square shape, at a certain moment this is not possible any more. Consequently, it is impossible to follow the etching process down to the substrate. A better method to investigate the length distribution of linear defects is to etch films of various thickness (see Sec. V A).

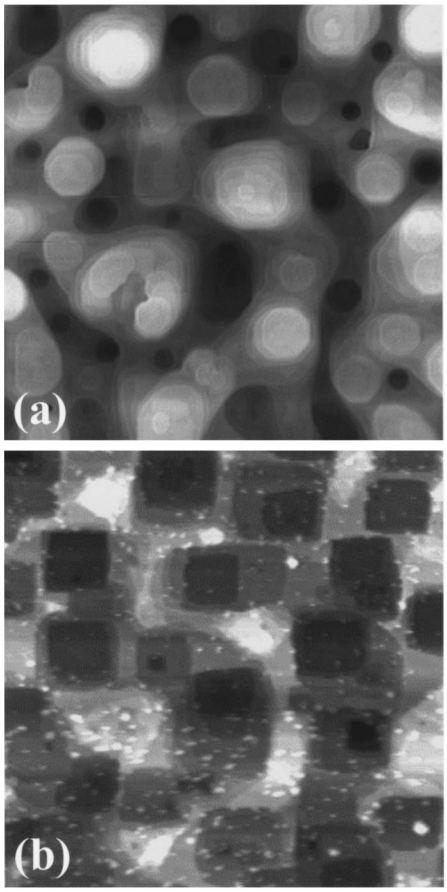

FIG. 4. AFM height images of a $YBa_2Cu_3O_{7-\delta}$ film laser deposited on (100) $SrTiO_3$ taken on the same position (scan size 2.0 μm): (a) as-grown surface morphology and (b) etched for 5 s. Every hole in the as-grown film surface corresponds to an etch pit, indicating that dislocations are situated around the growth islands. On the etched film surface some material is redeposited in the form of small precipitates.

Concluding, we find that the density of linear defects in $YBa_2Cu_3O_{7-\delta}$ films can be quantitatively determined by combining Br-ethanol etching with AFM. We identified some of the pits as being due to screw dislocations with a unit-cell Burgers vector. As etch pit formation is due to the stress energy within the dislocation core (and does not depend on the direction of the Burgers vector) both edge and screw dislocations with Burgers vectors of one unit cell or higher are revealed. Although in principle we can observe dislocations tilted with respect to the *c* axis, none of those were detected. Note that dislocations running parallel to the substrate are not revealed in our experiments.

IV. TUNING THE DISLOCATION DENSITY

Having a tool to determine dislocation densities, we investigate now the mechanism by which dislocations are induced during growth. Therefore we take a closer look at the position of the dislocations (or etch pits) with respect to the as-grown film surface. Figure 4 shows two AFM height images recorded directly after deposition and after etching the same film. Since these images are taken on the same position, we infer that dislocations are mainly situated *around*

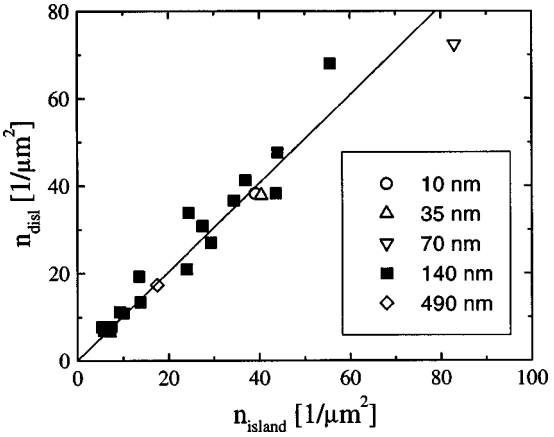

FIG. 5. Dislocation density n_{disl} as measured by etching as a function of the density of growth islands n_{island} of 10–490-nm-thick $YBa_2Cu_3O_{7-\delta}$ films laser deposited on (100) $SrTiO_3$ substrates. By manipulating n_{island} the number of dislocations can be tuned. The film thickness affects neither n_{disl} nor n_{island}.

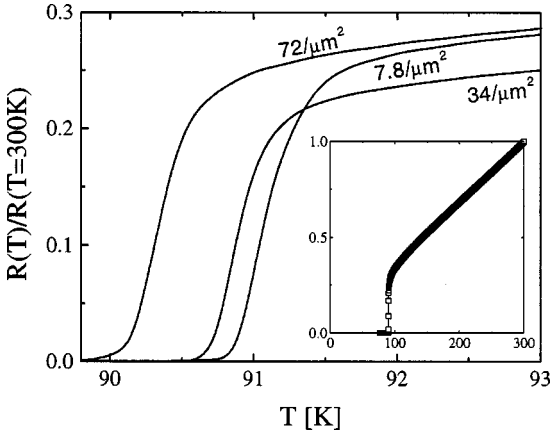

FIG. 6. Electrical resistance R as a function of temperature T for three $YBa_2Cu_3O_{7-\delta}$ films laser deposited on (100) $SrTiO_3$ with dislocation densities $n_{\mathrm{disl}}=7.8$, 34, and $72/\mu\mathrm{m}^2$; $R(T)$ is normalized with respect to $R(T=300\,\mathrm{K})$. The transition temperature T_c decreases with increasing n_{disl}. The inset shows $R(T)/R(T=300\,\mathrm{K})$ over a larger temperature range for the film with $n_{\mathrm{disl}}=72/\mu\mathrm{m}^2$. A typical value for the resistivity of films with intermediate n_{disl} is 83 $\mu\Omega$ cm at 100 K.

the islands in the holes in the trenches [in fact, this can also be seen in Figs. 2(b) and 3]. Apparently, surface depressions form at positions where dislocations emerge at the film surface. Indeed, Frank predicted[35] such depressions to form as a result of the strain energy associated with dislocations. However, the depressions in our films are much wider than predicted and they do not form around all dislocations.

To check the relation between the location of dislocations and the island structure, we deposited a series of $YBa_2Cu_3O_{7-\delta}$ films with various sizes of the growth islands. By increasing T_{sub} from 750 to 850 °C and p_{O2} from 15 to 50 Pa, the island diameter D can be varied reproducibly between 125 and 450 nm, respectively.[23] In Fig. 5 the dislocation density as measured by etching these films for ≈20 s in Br ethanol is plotted as a function of the density of growth island $n_{\mathrm{island}}=1/D^2$, showing that on average there is about one dislocation per island. By manipulating the island density the dislocation density can be varied reproducibly. In this way n_{disl} can be increased up to $68/\mu\mathrm{m}^2$. The range over which n_{disl} can be tuned is limited. As shown in Fig. 6, the superconducting transition temperature T_c decreases only slightly when increasing n_{disl}. Up to now, T_c could not be maintained above 90 K when decreasing the island size below 125 nm.

Films with various dislocation densities were used by Dam *et al.*[12] to prove that dislocations are responsible for the high critical currents in $YBa_2Cu_3O_{7-\delta}$ films. However, because of the one-to-one correspondence between islands (n_{island}) and dislocations (n_{disl}) the identification of the strongest pinning defect might be ambiguous. There could be other types of extended defects related to the island size. Two important experimental observations provide conclusive evidence that dislocations are the most important defects in these films. First of all, in sputtered films the relation between dislocation and island density does not hold: n_{island} is more than an order of magnitude smaller than n_{disl}. Yet, we find[12] that the characteristic field B^* is determined by the dislocation density. The second argument comes from PLD films themselves. It turns out that we can manipulate n_{island} by means of annealing the films for 30 min at temperatures around 800 °C in a flow of 97% Ar and 3% O_2 after deposition. As shown in Figs. 7(a) and 7(b), we observe a significant reconstruction of the film surface upon post annealing. The films not only become much flatter (rms roughness $R_q=2.1\rightarrow1.6$ nm), but also the size of the growth features in-

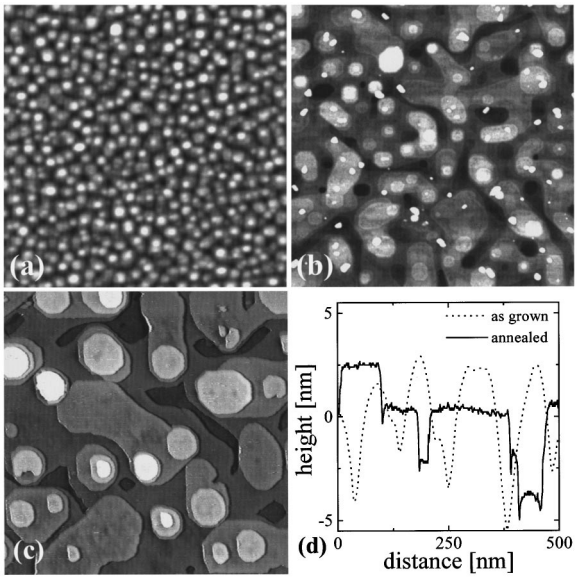

FIG. 7. Influence of post annealing on the surface morphology of a 41-nm-thick $YBa_2Cu_3O_{7-\delta}$ film laser deposited on (100) $SrTiO_3$ with a large island density. Shown are two AFM height images of $1.75\times1.75\,\mu\mathrm{m}^2$ (a) after deposition ($n_{\mathrm{island}}=105/\mu\mathrm{m}^2$) and (b) after post annealing the same film for 30 min at 800 °C in flowing Ar+3% O_2 ($n_{\mathrm{island}}=19/\mu\mathrm{m}^2$) and (c) an STM image of $1.00\times1.00\,\mu\mathrm{m}^2$ after post annealing. In (d) the typical height variations are shown as measured after deposition [AFM image (a)] and after the anneal treatment [STM image (c)]. Both n_{island} and the roughness are greatly reduced upon annealing. We note that upon annealing small off stoichiometries segregate to the film surface and form small secondary phases, as can be seen in (b).

creases drastically (leading to a drastic decrease of their density: $n_{island}=105\rightarrow 19/\mu m^2$). To illustrate these points, in Fig. 7(c) an STM image of the surface morphology after post annealing is shown. Interestingly, the step height of the islands after post annealing is exactly equal to two $YBa_2Cu_3O_{7-\delta}$ unit cells (2.4 nm), see Fig. 7(d).

Since the dislocation density as measured by etching does *not change as much as* the island density upon post annealing,[36] the relation between n_{island} and n_{disl} (Fig. 5) is lost. Yet, B^* remains determined by n_{disl} and not by n_{island}.[36] We conclude that dislocations are the most important source for strong pinning in $YBa_2Cu_3O_{7-\delta}$ films.

We note that post annealing only has an effect on the surface morphology (n_{island}) if the anneal temperature is *higher* than the applied deposition temperature. It is the highest temperature that determines the surface diffusion distance and therefore the resulting surface morphology. Our post-anneal experiments also indicate that the relation between growth morphology and etch pit density depends on the growth parameters. For instance, if one chooses a lower deposition rate some of the post annealing will already occur during deposition, yielding a decrease of the islands density with film thickness. This may also explain the fact that some authors observe an increase of the island size with the film thickness.[37]

V. DISLOCATION DISTRIBUTION

At this point we are not only able to quantitatively determine dislocation densities, but we can also tune their density. In this section both the length (along the *c* axis of $YBa_2Cu_3O_{7-\delta}$) and lateral (in the *ab* plane) distribution of the growth-induced linear defects are investigated as a function of the defect density.

A. Length distribution

So far, we determined dislocation densities at or close to the film surface. In order to investigate the *length* distribution of dislocations, a series of films was grown with a thickness of 10, 35, 70, and 490 nm. These films exhibit the same characteristic island structure as in Fig. 2(a), even for films as thin as 10 nm (see Fig. 8 for an example). Etching these films and plotting the results in Fig. 5, we find that the relation between islands and dislocations does not depend on the film thickness. This observation indicates that n_{island} and therefore also n_{disl} do not depend on the film thickness. Since dislocation cannot end inside a crystal,[17] this implies that dislocations have to run through the entire film thickness. Hence they must be formed at the substrate-film interface. Therefore the distribution of dislocation lengths is uniform: all dislocations have a length comparable to the film thickness.[38] Indeed, TEM studies[39] on laser ablated $YBa_2Cu_3O_{7-\delta}$ on (100) $SrTiO_3$ substrates revealed dislocations with a density of the order of $10/\mu m^2$ that extend from the interface towards the film surface.

B. Lateral distribution

As dislocations are situated around the growth islands (Fig. 4), the in-plane defect distribution is not completely random. To quantify this short-range ordering, we determined the radial dislocation distribution function $g(r)$ from the etch pit distribution[40] as measured by AFM. Taking a certain etch pit as a reference point, we count the number of pits $\Delta N(r)$ within a ring of width Δr at a distance r. Then, $g(r)=\Delta N(r)/(2n_{disl}\pi r\Delta r)$. This procedure is repeated with every dislocation as a reference dislocation and finally averaged. In order to improve the statistics, periodic boundary conditions are used (the results are not influenced by the use of periodic boundary conditions). The outcome of this statistical analysis is shown in Fig. 9 for three films with dislocation densities of 7.8, 34, and $68/\mu m^2$.

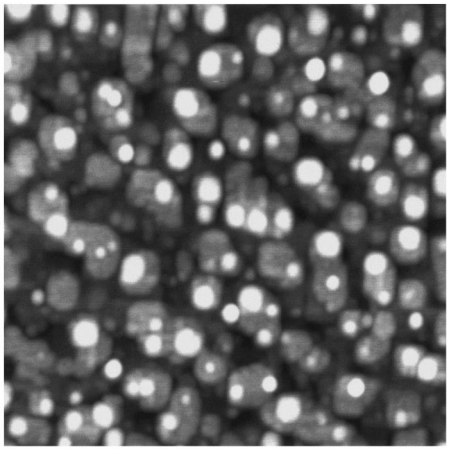

FIG. 8. AFM height image of a 10-nm-thick $YBa_2Cu_3O_{7-\delta}$ film laser deposited on (100) $SrTiO_3$ with an island density of $70/\mu m^2$, indicating that the familiar morphology is already formed after depositing a few monolayers of $YBa_2Cu_3O_{7-\delta}$. The image size is $1.0\times 1.0\ \mu m^2$.

By normalizing r with respect to the average dislocation spacing d_{disl} ($=1/\sqrt{n_{disl}}$), all curves scale onto a single radial distribution function $g(r/d_{disl})$, indicating that the distribution is universal. For comparison, the result for a random distribution [$g(r)=1$] is included. We note that the decrease of $g(r)$ for small r is *not* an artifact of the analysis. By etching films very shortly, we are able to distinguish etch pits

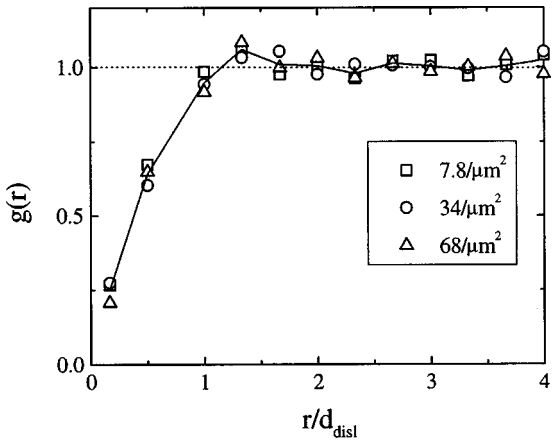

FIG. 9. Radial dislocation distribution function $g(r)$ of three $YBa_2Cu_3O_{7-\delta}$ films laser deposited on (100) $SrTiO_3$ with dislocation densities $n_{disl}=7.8$, 34, and $68/\mu m^2$. By normalizing the radial coordinate r with respect to the average dislocation spacing $d_{disl}=1/\sqrt{n_{disl}}$, the function $g(r/d_{disl})$ scales onto a universal curve; $g(r)=1$ for a random distribution (dotted line).

that are only 30 nm apart. Moreover, because of the characteristic square shape even overlapping etch pits can be resolved. Obviously, the statistics become poor at small r and we estimate the lower limit of our analysis to be 50 nm, which corresponds to $r/d_{\mathrm{disl}}=0.41$, 0.29, and 0.14 for $n_{\mathrm{disl}}=7.8$, 34, and $68/\mu\mathrm{m}^2$, respectively. The most striking difference between the measured defect distribution and a random distribution (Fig. 9) is found at small distances, $r<d_{\mathrm{disl}}$. Below the average dislocation spacing, there is only a small chance to find another dislocation, pointing to short-range ordering of the defects. In the next section we will discuss the origin of this self-organization of defects in more detail.

C. Implications for vortex pinning

The fact that dislocations run from the substrate-film interface up to the film surface is highly favorable for the pinning of vortices. This is the main reason for large critical current densities up to $10^{12}\,\mathrm{A/m}^2$ in $YBa_2Cu_3O_{7-\delta}$ films in magnetic fields below B^*.[12,13] The self-organization of dislocations results in a more efficient occupation of the strong pinning sites by vortices. For a given density of defects, the critical current remains constant up to higher fields than for randomly distributed columnar defects created by means of heavy-ion irradiation.[12]

Moreover, the short-range ordering of the defect structure could make these films a good candidate for observing the Mott-insulator vortex phase,[3,20] which was predicted to occur at low temperatures when the applied magnetic field ($\| c$ axis) exactly equals the matching field $B_\Phi \equiv n_{\mathrm{disl}}\Phi_0$. In this situation all linear defects are occupied by exactly one vortex. Consequently, introducing another vortex requires a large energy. Therefore both a characteristic jump in the (reversible) magnetization as well as a diverging tilt and compression modulus of the vortex lattice are expected. So far, however, only remnants of these characteristics have been observed.[41] As was numerically shown by Wengel and Täuber,[41,42] this is not surprising because the true Mott-insulator phase is only expected for (i) weakly interacting vortices, i.e., when the average defect spacing d_{disl} is considerably larger than the magnetic penetration depth λ ($\lambda/d_{\mathrm{disl}}\rightarrow 0$) and (ii) for a regular array of columnar defects. Since in our films the defect distribution exhibits short-range ordering, the latter condition is much better satisfied than for randomly distributed columnar defects in irradiated single crystals. What about the first condition? The smallest dislocation density obtained thus far is $7.8/\mu\mathrm{m}^2$, corresponding to $d_{\mathrm{disl}}=358\,\mathrm{nm}$, i.e., much larger that the *bulk ab*-penetration depth at zero temperature $\lambda_{ab}(0)=145\,\mathrm{nm}$.[43] Yet, we did not observe the predicted characteristic jump in the magnetization. However, in thin films one should compare d_{disl} to the *effective*[44] penetration depth $\Lambda\approx 2\lambda^2/t$, where t is the film thickness, which is significantly larger ($\Lambda\approx 300\,\mathrm{nm}$ for $t=140\,\mathrm{nm}$). Therefore in order to observe the Mott insulator phase, one should (i) decrease Λ by depositing thicker films and (ii) increase d_{disl} by depositing films with lower dislocation densities (using $T_{\mathrm{sub}}>850\,^\circ\mathrm{C}$). As in our films both the length and the radial distribution do not depend on the film thickness (for $10<t<490\,\mathrm{nm}$) nor on the defect density (for $7.8<n_{\mathrm{disl}}<68/\mu\mathrm{m}^2$), it will be meaningful to search for the Mott-insulator phase in thick laser ablated $YBa_2Cu_3O_{7-\delta}$ films with a low density of natural linear defects.

VI. MECHANISMS OF DISLOCATION FORMATION

In the previous section, it was shown that dislocations are introduced in the early stages of growth at the substrate-film interface. In this section we address the question how dislocations are generated. Generally, the mechanisms for dislocation formation in thin films are either substrate related or related to the growth of $YBa_2Cu_3O_{7-\delta}$ itself. We consider here three possible mechanisms:[45]

(i) *Inheritance of dislocations*:[32,46] Linear defects in the $SrTiO_3$ substrate may be reproduced by the $YBa_2Cu_3O_{7-\delta}$ film deposited on it.

(ii) *Release of misfit strain*:[47] The lattice mismatch between substrate and film induces strain during the growth of $YBa_2Cu_3O_{7-\delta}$ films. Since the elastic strain energy increases with film thickness, it is expected that this strain is released by introducing dislocations above a certain critical thickness t_c.[48]

(iii) *Merging of misaligned growth fronts*:[46,47] During deposition, growth fronts of different heights/orientation can merge, resulting in the formation of a dislocation. Within this mechanism we can distinguish[49] coalescence of two different growth fronts and recombination of the same growth front. The latter process occurs when growth fronts flow over small irregularities, for instance, off-stoichiometric precipitates.

These mechanisms are discussed in more detail below.

A. Inheritance from the substrate

As Eissler, Wang, and Dietsche[32] suggested that dislocations are inherited from the substrate, we determined the dislocation density in $SrTiO_3$ substrates by means of etching in 1 HF: 2 HNO_3: 2 H_2O. Analogous to the etching of $YBa_2Cu_3O_{7-\delta}$ films, etch pits form at linear defect sites. In Fig. 10 AFM images of two different $SrTiO_3$ substrates are shown after etching (note the large scales), giving an idea of the range of dislocation densities that can be found in the substrate material. Usually, we find densities that are three orders of magnitude smaller ($10^{-2}/\mu\mathrm{m}^2$) than those in the films ($10/\mu\mathrm{m}^2$); see Fig. 10(a). The highest dislocation density observed in substrates so far [about $1/\mu\mathrm{m}^2$; see Fig. 10(b)], is still smaller than the lowest dislocation density achieved in films, indicating that inheritance is not the main origin of dislocations in films. Although we cannot rule inheritance out, in general, the film seems to be insensitive to the substrate defect structure.

This is again shown when we artificially create linear defects in the $SrTiO_3$ substrate by bombarding it with 500-keV Xe^{4+} (with a dose of $200/\mu\mathrm{m}^2$). $YBa_2Cu_3O_{7-\delta}$ films grown on these bombarded substrates, all show the expected dislocation densities ($10/\mu\mathrm{m}^2$) rather than the implanted dose in the substrate (we checked that the linear defects due to implantation were still present after film deposition by etching off the film and subsequently etching the substrate). We con-

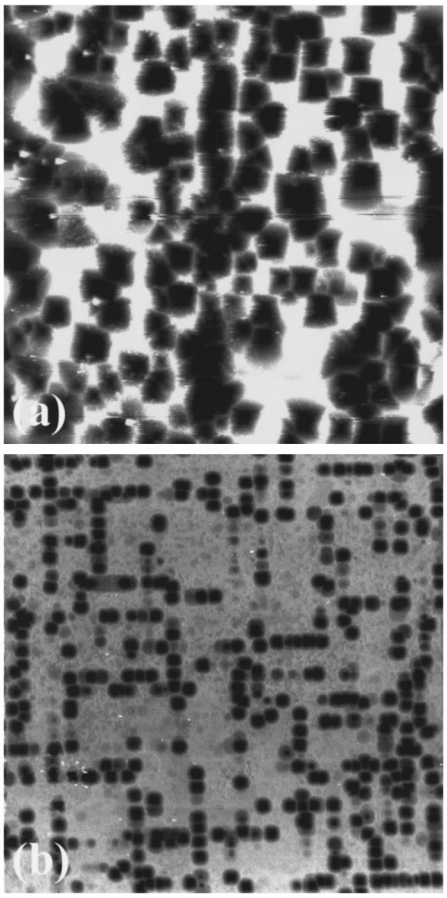

FIG. 10. AFM height images of two (100) $SrTiO_3$ substrates, etched for 30 s in a 1 HF:2 HNO_3:2 H_2O solution, showing the spread in dislocation density n_{disl} between different substrates: (a) a typical substrate with $n_{disl}=10^{-2}/\mu m^2$ (image size 100 $\times 100\,\mu m^2$) and (b) a ''bad'' substrate with $n_{disl}=1/\mu m^2$ (image size $20\times 20\,\mu m^2$).

clude that the linear defects in the film are due to the $YBa_2Cu_3O_{7-\delta}$ growth process and are relatively insensitive to the surface properties of the substrate.

B. Release of misfit strain

Another possibility for the formation of dislocations at the interface is the relaxation of strain, originating from the mismatch between substrate and film. Generally, a film may release this strain either by introducing misfit dislocations[47] or by forming cracks.[50] Clearly, crack formation does not take place in our $YBa_2Cu_3O_{7-\delta}$ films and we will concentrate on the formation of misfit relieving dislocations. Because the substrate-film mismatch is in the *ab* plane, the mechanism leading to the creation of dislocations along the *c* axis is not *a priori* clear. It has been suggested[47,48] that dislocation half loops created at the film surface glide towards the substrate-film interface to form strain relieving misfit dislocations. The dislocation segments left at each end of the misfit dislocation thread the film (parallel to the *c* axis).[51] However, energetically this mechanism is very unfavorable because of the large Burgers vector involved.[45] Also, this mechanism cannot explain why the number of dislocations created at the interface decreases substantially when growing a film with larger islands, i.e., at higher substrate temperatures. Given the large activation energy associated with the formation of half loops,[45] one would rather expect a larger number of loops (and thus a larger number of threading dislocations) at higher deposition temperatures. Moreover, we do not observe the merging of etch pits upon repeated etching or any other sign that they originate from dislocation half loops. Another argument against this mechanism is the fact that also in films as thin as 10 nm (see Fig. 8) dislocations are observed. These thin films are expected to grow strained, without relaxation, since the energy to form a dislocation is larger than the elastic energy gain. For $YBa_2Cu_3O_{7-\delta}$ on $SrTiO_3$ the critical thickness t_c at which this occurs was estimated to be 20 nm,[48] i.e., considerably thicker than the 10-nm thin film investigated here.

The most convincing argument, however, against the influence of the substrate mismatch on n_{disl} is found in $YBa_2Cu_3O_{7-\delta}$ films deposited on (100) MgO substrates. Since the mismatch between $YBa_2Cu_3O_{7-\delta}$ and MgO is about 9%, i.e., much larger than the mismatch with $SrTiO_3$ (1.5%), more strain relieving dislocations are needed when using MgO substrates. Indeed, dislocation densities up to $10^3/\mu m^2$ have been revealed by transmission electron microscopy (TEM) of $YBa_2Cu_3O_{7-\delta}$ films on MgO.[52] In Fig. 11, AFM images of the surface morphology of two $YBa_2Cu_3O_{7-\delta}$ films laser deposited on MgO with different dislocation densities are shown. It turns out that also on MgO the dislocation density can be decreased by increasing T_{sub} and/or p_{O2}, analogous to films deposited on $SrTiO_3$. Also, the surface morphology of films grown on $SrTiO_3$ (Fig. 2) and on MgO [Fig. 11(a)] is comparable. A clear island structure is again observed and no indication of spiral outcrops is found. Upon etching, etch pits form with a density equal to the island density [Fig. 11(b)], indicating that no additional dislocations along the *c* axis are created as compared to films on $SrTiO_3$. Misfit may induce in-plane dislocations. However, these dislocations do not influence the characteristic field dependence of the critical current density,[12] when the applied field is parallel to the *c* axis. Etching $YBa_2Cu_3O_{7-\delta}$ films deposited at high substrate temperatures (small n_{disl} on MgO) reveals the presence of additional grain boundaries [(Figs. 11(c) and 11(d)]. The amount of grain boundaries increases with increasing substrate temperature. Since the edges of the etch pits are always parallel to the [100] and [010] directions of $YBa_2Cu_3O_{7-\delta}$ (see Sec. III A), the orientation of etch pits in the different grains in Fig. 11(d) implies that these are 45° grain boundaries. Indeed, 45° in plane rotationally misaligned $YBa_2Cu_3O_{7-\delta}$ domains have been observed on MgO (Ref. 53) at a density that increases with the substrate temperature.[54] We note that these grain boundaries may consist of dislocations, thereby explaining the high densities of dislocations that were observed by TEM.[52]

Apart from the introduction of grain boundaries at high substrate temperatures, the use of a larger mismatched substrates does not induce additional growth dislocations. We conclude that the release of misfit strain is not the main mechanism for introducing dislocations along the *c* axis of the film.

C. Merging of misaligned growth fronts

Since the defect density can be tuned by means of the deposition conditions, we expect that the mechanism for dis-

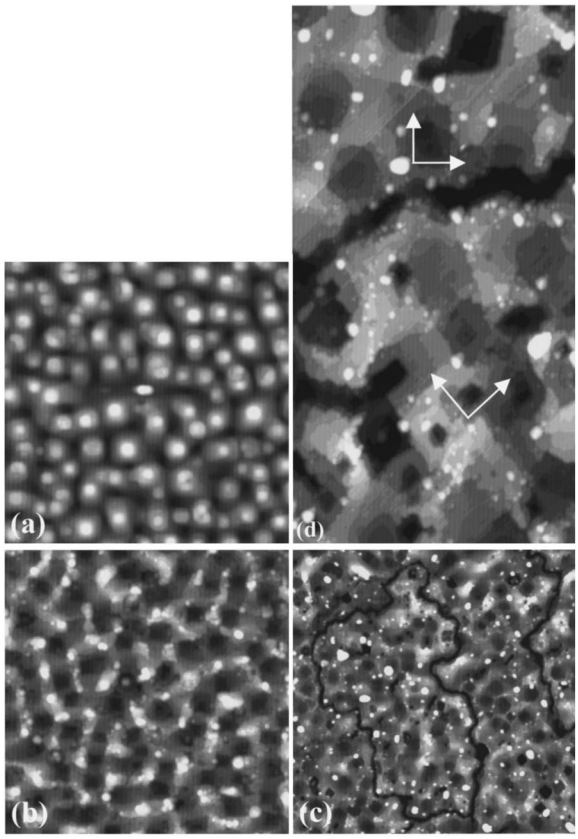

FIG. 11. AFM height images of two $YBa_2Cu_3O_{7-\delta}$ films laser deposited on (100) MgO substrates with a high ($n_{disl}=24/\mu m^2$) and a low ($n_{disl}=8/\mu m^2$) dislocation density. The thickness of film with a high n_{disl} shown in (a) and (b) is 160 nm, while the film with a low n_{disl} in (c) and (d) is 100 nm thick: (a) as-grown surface morphology ($n_{island}=27/\mu m^2$, image size $3.0\times3.0\ \mu m^2$), (b) same film but now etched for 25 s and (c) the low dislocation density film after etching for 25 s, showing that grain boundaries are also revealed (image size $5.0\times5.0\ \mu m^2$). In (d) a closeup ($1.07\times2.04\ \mu m^2$) of a high-angle grain boundary in (c) is shown; the 45° rotation of etch pits across the boundary is clarified by arrows.

location formation is closely related to the first stages of heteroepitaxial growth. It has been suggested that dislocations are induced when misaligned growth fronts meet,[46,47] for instance, at the intersection of nuclei that originated a nonintegral number of unit cells away from each other.[55] Thus coalescence of the first layer of growth islands can yield dislocations that persist all the way up to the film surface.

There are a number of experimental arguments which are in favor of such an island coalescence mechanism. First of all, the tunability of the dislocation density by means of the island density. Lowering the deposition temperature, results in a reduced surface mobility of the impinging atom species. As a result, the number of nuclei increases and, correspondingly, the number of island coalescence events, generating more dislocations.

In fact, any growth process that generates misaligned growth fronts could, in principle, act as a source for dislocations. Therefore also precipitates can well be the cause of such misalignment. Since the dislocations form close to the substrate, this means that such secondary phases have to form preferentially during the growth of the first monolayers of $YBa_2Cu_3O_{7-\delta}$. This might well be the case, since in heteroepitaxial growth the nature of the nucleus is determined by a delicate balance of surface/interface energy and crystallization energy.[31] It has been observed both by *in situ* STM (Ref. 56) and TEM (Refs. 57 and 58) that the first monolayer consists of a phase different from $YBa_2Cu_3O_{7-\delta}$ on $SrTiO_3$. In that case, the remaining constituents tend to form precipitates, presumably Y_2O_3 or CuO.[59] Indeed, Matijasevic *et al.*[59] observed a high density of precipitates when depositing less than a monolayer of $SmBa_2Cu_3O_{7-\delta}$ (123) on $SrTiO_3$ by means of molecular-beam epitaxy. They could reduce the precipitate density significantly by properly adjusting the 123 composition of the first monolayer towards a 1:3:3 cation stoichiometry. Also, TEM observations[60] on one-unit-cell-thick $YBa_2Cu_3O_{7-\delta}$ films grown on (001) Y-ZrO_2 substrates by pulsed laser depositions show preferential formation of CuO precipitates in the initial growth stages. Such precipitates obstruct the propagation of a growth front, leading to the merging of two misaligned branches of the same growth when they are overgrown (see for instance Fig. 7 in Ref. 45 or Fig. 6 in Ref. 49). Consequently, it is likely that dislocations form at precipitate sites. In the scenario of precipitate induced dislocations, the temperature dependence of the dislocation density is explained in terms of the segregation kinetics of the precipitates. At lower temperatures, the spacing between precipitates is smaller due to the smaller surface diffusion distance, resulting in a higher precipitate density (higher dislocation density). The self-organization of dislocations can be understood by assuming that the kinetics are diffusion controlled.

We have therefore two mechanisms, i.e., dislocations induced by overgrowing precipitates or by islands coalescence, which are potentially leading to the observed phenomena. In order to decide which mechanism is dominant we started investigating ultrathin films. In Fig. 12(a) an AFM image of a $YBa_2Cu_3O_{7-\delta}$ film with a thickness slightly over one unit cell (u.c.) is shown. The substrate is fully covered with one monolayer of $YBa_2Cu_3O_{7-\delta}$ (or a related phase[56–59]). Embedded in this matrix, we observe a significant number of precipitates ($22/\mu m^2$). As shown in Fig. 12(b), these precipitates are absent in films of 4 u.c. in thickness. Apparently, these precipitates are characteristic for the first layer only. Now, these secondary phases may generate dislocations when the are overgrown. The density of precipitates is larger than the dislocation density expected for a thicker $YBa_2Cu_3O_{7-\delta}$ film deposited under the same deposition conditions ($7.8/\mu m^2$). However, we should stress that not all precipitates necessarily generate dislocations when they are overgrown.

To prove that precipitates can generate dislocations, we deposited small particles from a Y_2O_3 target on a bare $SrTiO_3$ substrate prior to the actual film deposition, see Fig. 13. In this figure Y_2O_3 precipitates can be distinguished with a density of $54/\mu m^2$. Now depositing a $YBa_2Cu_3O_{7-\delta}$ film over this precipitate structure at a substrate temperature of 850 °C, yields a dislocation density of $41/\mu m^2$. This is more than five times larger than the dislocation density in films deposited under identical condition on clean substrates ($7.8/\mu m^2$) and we conclude that precipitates serve as nucleation sites for dislocations.

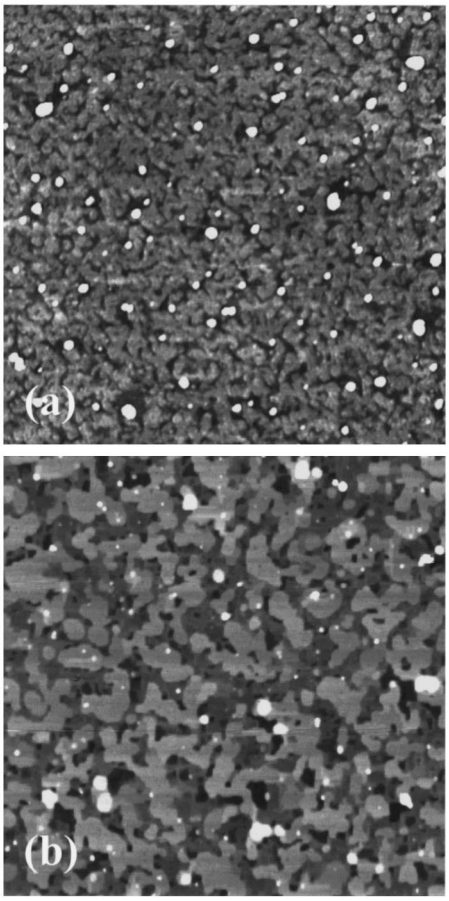

FIG. 12. AFM height images ($2.0\times2.0\,\mu m^2$) of two ultrathin YBaCuO films laser deposited on (100) $SrTiO_3$: (a) one monolayer, showing precipitates ($22/\mu m^2$) embedded in the first monolayer and (b) four monolayers, indicating that precipitates are absent or overgrown.

Summarizing, we have shown that (i) preferential precipitation takes place in the first stages of $YBa_2Cu_3O_{7-\delta}$ growth and (ii) Y_2O_3 precipitates induce additional dislocation. These are strong indications that dislocations are not formed as a result of coalescence of the first growth islands but that they are induced by the precipitates that form preferentially in the first monolayer. However, we did not yet observe the creation of dislocation when such precipitates are overgrown. To reveal the details of this dislocation formation mechanism we are presently carrying out cross sectional TEM studies and *in situ* AFM/STM measurements on ultrathin $YBa_2Cu_3O_{7-\delta}$ films.

VII. CONCLUSIONS

Since dislocations are the most important flux pinning centers in $YBa_2Cu_3O_{7-\delta}$ films deposited on (100) $SrTiO_3$ substrates,[12] it is of great interest to understand the mechanism by which these dislocations are induced. We developed a repetitive wet-chemical etching technique which enables us to determine the density of all dislocations (edge, screw, and mixed character) when combined with atomic force microscopy. It turns out that also high-angle grain boundaries are resolved by this technique.

By etching laser-ablated films with a thickness ranging from 490 down to 10 nm, we find that dislocations are induced at the substrate-film interface. Consequently, dislocations must be induced either by the substrate itself (by inheritance of defects from the substrate or by release of the substrate-film misfit strain) or during the first stages of growth when misaligned growth fronts merge.

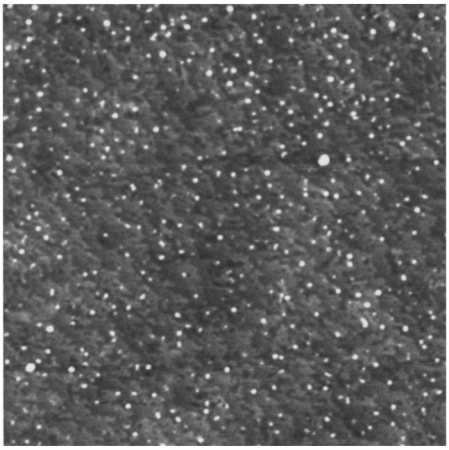

FIG. 13. AFM height image ($3.0\times3.0\,\mu m^2$) of Y_2O_3 precipitates laser deposited on a (100) $SrTiO_3$ substrate. The density of Y_2O_3 precipitates is $54/\mu m^2$. The vicinal steps in the substrate of 0.4 nm in height are along the [110] direction and are separated 177 nm, corresponding to a miscut angle of 0.13°.

It is shown that linear defects in the substrate and the misfit between substrate and film are *not* the origin of dislocation formation. We propose that dislocations form as a result of the merging of misaligned $YBa_2Cu_3O_{7-\delta}$ growth fronts when overgrowing precipitates which are formed in the first monolayer only. These precipitates are a result of the peculiarities of the nucleation mechanism of $YBa_2Cu_3O_{7-\delta}$ on $SrTiO_3$. Indeed, precipitation is observed during growth of the first monolayer of $YBa_2Cu_3O_{7-\delta}$ on $SrTiO_3$ with a density of the order of the expected dislocation density. It is also shown that artificially induced precipitates create additional dislocations, indicating that such a dislocation generation mechanism is indeed operative.

Since dislocations can only end at interfaces, they persist up to the film surface parallel to the *c* axis, resulting in a uniform length distribution. As the dislocations are mainly situated *around* growth islands, we can reproducibly tune the density of dislocations between 5 and $70/\mu m^2$ by manipulating the size of the growth features. To obtain a certain defect density we only need to adjust the substrate temperature and oxygen background pressure. At higher temperatures the larger surface diffusivity results in a lower density of precipitates, generating less dislocations.

Statistical analysis of the lateral defect distribution of films with various dislocation densities shows that the radial dislocation distribution function $g(r)$ can be scaled onto a single curve $g(r/d_{\mathrm{disl}})$, where d_{disl} is the average dislocation spacing. Both the length as well as the radial dislocation distribution do not depend on the density of defects nor on the film thickness. Interestingly, $g(r/d_{\mathrm{disl}})$ approaches zero for small distances $r<d_{\mathrm{disl}}$, indicating that the defect distribution exhibits short-range ordering. We attribute this self-organization to the presence of diffusion fields around the precipitates.

In conclusion, we have identified the nature of strong pinning defects in $YBa_2Cu_3O_{7-\delta}$ in films. Pinning is due to dislocations formed at the substrate-film interface. We can enhance the density of pinning sites by decreasing the substrate temperature or by depositing a layer of Y_2O_3 precipitates before starting the $YBa_2Cu_3O_{7-\delta}$ growth process. In contrast to the artificial columnar defects created by means of heavy-ion irradiation, in thin films the strong pinning linear defects exhibit a nonrandom spatial distribution. Both the tunability of the defect density and the self-organization of defects show that films are very attractive for studying vortex matter. If we are also able to influence the *distribution* of dislocations, for instance, by depositing a regular lattice of precipitates prior to the actual film growth, it may be possible to observe the predicted Mott-insulator vortex phase.

ACKNOWLEDGMENTS

The authors thank S. Freisem and J. Aarts (Kamerlingh Onnes Laboratory, Leiden University, The Netherlands) for supplying us with sputtered $YBa_2Cu_3O_{7-\delta}$ films. Use of the ion implantation facility at the AMOLF-FOM institute in Amsterdam is gratefully acknowledged. This work is part of the research program of FOM (stichting Fundamenteel Onderzoek der Materie), which is financially supported by NWO (stichting Nederlands Wetenschappelijk Onderzoek).

*Author to whom correspondence should be addressed. Electronic address: dam@nat.vu.nl

[1] L. Civale, A. D. Marwick, M. W. McElfresh, T. K. Worthington, A. P. Malozemoff, F. H. Holtzberg, J. R. Thompson, and M. A. Kirk, Phys. Rev. Lett. **65**, 1164 (1990).
[2] T. L. Hylton and M. R. Beasley, Phys. Rev. B **41**, 11 669 (1990).
[3] D. R. Nelson and V. M. Vinokur, Phys. Rev. B **48**, 13 060 (1993).
[4] G. Blatter, M. V. Feigel'man, V. B. Geshkenbein, A. I. Larkin, and V. M. Vinokur, Rev. Mod. Phys. **66**, 1125 (1994).
[5] T. Haage, J. Zegenhagen, J. Q. Li, H.-U. Habermeier, M. Cardona, Ch. Jooss, R. Warthmann, A. Forkl, and H. Kronmüller, Phys. Rev. B **56**, 8404 (1997).
[6] J. Mannhart, D. Anselmetti, J. G. Bednorz, A. Catana, Ch. Gerber, K. A. Müller, and D. G. Schlomm, Z. Phys. B: Condens. Matter **86**, 177 (1992).
[7] H. Douwes, P. H. Kes, Ch. Gerber, and J. Mannhart, Cryogenics **33**, 486 (1993).
[8] F. C. Klaassen, J. M. Huijbregtse, B. Dam, R. van der Geest, G. Doornbos, J. H. Rector, R. Elberse, and R. Griessen, in *Physics and Materials Science of Vortex States, Flux Pinning and Dynamics*, edited by R. Kossowsky, S. Bose, V. Pan, and Z. Durusoy (Kluwer Academic, Dordrecht, 1999).
[9] Ch. Jooss, A. Forkl, R. Warthmann, H.-U. Habermeier, B. Leibold, and H. Kronmüller, Physica C **266**, 235 (1996).
[10] D. H. Lowndes, D. K. Christen, C. E. Klabunde, Z. L. Wang, D. M. Kroeger, J. D. Budai, Shen Zhu, and D. P. Norton, Phys. Rev. Lett. **74**, 2355 (1995).
[11] A. Díaz, L. Mechin, P. Berghuis, and J. E. Evetts, Phys. Rev. Lett. **80**, 3855 (1998).
[12] B. Dam, J. M. Huijbregtse, F. C. Klaassen, R. C. F. van der Geest, G. Doornbos, J. H. Rector, A. M. Testa, S. Freisem, J. C. Martinez, B. Stäuble-Pümpin, and R. Griessen, Nature (London) **399**, 439 (1999).
[13] F. C. Klaassen, G. Doornbos, J. M. Huijbregtse, R. C. F. van der Geest, B. Dam, and R. Griessen (unpublished).
[14] Ch. Gerber, D. Anselmetti, J. G. Bednorz, J. Mannhart, and D. G. Schlomm, Nature (London) **350**, 279 (1991).
[15] M. Hawley, I. D. Raistrick, J. G. Beery, and R. J. Houlton, Science **251**, 1587 (1991).
[16] B. Dam, N. J. Koeman, J. H. Rector, B. Stäuble-Pümpin, U. Poppe, and R. Griessen, Physica C **261**, 1 (1996).
[17] D. Hull, *Introduction to Dislocations* (Pergamon, Oxford, UK, 1975).
[18] L. Civale, A. D. Marwick, T. K. Worthington, M. A. Kirk, J. R. Thompson, L. Krusin-Elbaum, Y. Sun, J. R. Chem, and F. Holtzberg, Phys. Rev. Lett. **67**, 648 (1991).
[19] L. Civale, Supercond. Sci. Technol. **10**, A11 (1997).
[20] D. R. Nelson and V. M. Vinokur, Phys. Rev. Lett. **68**, 2398 (1992).
[21] B. Dam, J. Rector, M. F. Chang, S. Kars, D. G. de Groot, and R. Griessen, Appl. Surf. Sci. **86**, 13 (1995).
[22] J. M. Huijbregtse, B. Dam, J. H. Rector, and R. Griessen, J. Appl. Phys. **86**, 6528 (1999).
[23] B. Dam, J. H. Rector, J. M. Huijbregtse, and R. Griessen, Physica C **305**, 1 (1998).
[24] S. Freisem, A. Brockhoff, D. G. de Groot, B. Dam, and J. Aarts, J. Magn. Magn. Mater. **165**, 380 (1997).
[25] R. B. Heimann, in *Auflösung von Kristallen*, edited by V. D. Fréchette, H. Kirsch, L. B. Sand, and F. Trojer (Springer-Verlag, Vienna, Austria, 1975).
[26] R. P. Vasquez, B. D. Hunt, and M. C. Foote, Appl. Phys. Lett. **53**, 2692 (1988).
[27] A. Roshko, S. E. Russek, K. A. Trott, S. C. Sanders, M. E. Johansson, J. S. Martens, and D. Zhang, IEEE Trans. Appl. Supercond. **5**, 1733 (1995).
[28] F. Miletto Granozio, U. Scotti di Uccio, M. Valentino, G. G. Condorelli, I. L. Fragalà, and G. Malandrino, Physica C **271**, 83 (1996).
[29] C. T. Lin and W. Y. Liang, Physica C **225**, 275 (1994).
[30] F. R. N. Nabarro, *Theory of Crystal Dislocations* (Oxford University Press, Oxford, Great Britain, 1967).
[31] B. Dam and B. Stäuble-Pümpin, J. Mater. Sci.: Mater. Electron. **9**, 217 (1998).
[32] D. Eissler, H. S. Wang, and W. Dietsche, Appl. Phys. Lett. **62**, 1292 (1993).
[33] L. E. C. van de Leemput, P. J. M. van Bentum, F. A. J. M. Driessen, J. W. Gerritsen, H. van Kempen, and L. W. M. Scheurs, J. Cryst. Growth **98**, 551 (1989).
[34] H. P. Lang, H. Haefke, G. Leemann, and H.-J. Güntherodt, Physica C **194**, 81 (1992).
[35] F. C. Frank, Acta Crystallogr. **4**, 498 (1951).
[36] J. M. Huijbregtse, F. C. Klaassen, A. Szepielow, B. Dam, and R. Griessen (unpublished).
[37] D. H. A. Blank, M. E. Bijlsma, R. Moerman, H. Rogalla, F. J. B. Stork, and A. Roshko, J. Alloys Compd. **251**, 31 (1997).
[38] In our previous paper (Ref. 12), we employed the repetitive etching technique to determine the dislocation length distribution. There, we did not take the effect of overlapping etch pits into account, resulting in an underestimation of the number of defects created at the substrate-film interface. However, in our analysis we took n_{disl} equal to the etch pit density as measured at the surface. Therefore the contents of this paper are not affected.

[39] O. Eibl and B. Roas, J. Mater. Res. **5**, 2620 (1990).
[40] D. Rose, K. Durose, W. Palosz, A. Szczerbakow, and K. Grasza, J. Phys. D **31**, 1009 (1998).
[41] C. Wengel and U. C. Täuber, Phys. Rev. Lett. **78**, 4845 (1997).
[42] C. Wengel and U. C. Täuber, Phys. Rev. B **58**, 6565 (1998).
[43] J. E. Sonier, R. F. Kiefl, J. H. Brewer, D. A. Bonn, J. F. Carolan, K. H. Chow, P. Dosanjh, W. N. Hardy, Ruixing Liang, W. A. MacFarlane, P. Mendels, G. D. Morris, T. M. Riseman, and J. W. Schneider, Phys. Rev. Lett. **72**, 744 (1994).
[44] E. H. Brandt, Rep. Prog. Phys. **58**, 1465 (1995).
[45] B. Stäuble-Pümpin, V. C. Matijasevic, B. Ilge, J. E. Mooij, W. J. A. M. Peterse, P. M. L. O. Scholte, F. Tuinstra, H. J. Venvik, D. S. Wai, C. Traeholt, J. G. Wen, and H. W. Zandbergen, Phys. Rev. B **52**, 7604 (1995).
[46] D. G. Schlomm, D. Anselmetti, J. G. Bednorz, R. F. Broom, A. Catana, T. Frey, Ch. Gerber, H.-J. Günterhodt, H. P. Lang, and J. Mannhart, Z. Phys. B: Condens. Matter **86**, 163 (1992).
[47] S. J. Pennycook, M. F. Chisholm, D. E. Jesson, R. Feenstra, S. Zhu, X. Y. Zheng, and D. J. Lowndes, Physica C **202**, 1 (1992).
[48] M. Yeadon, M. Aindow, F. Wellhöfer, and J. S. Abell, J. Cryst. Growth **172**, 145 (1997).
[49] D. G. Schlomm, D. Anselmetti, J. G. Bednorz, Ch. Gerber, and J. Mannhart, J. Cryst. Growth **137**, 259 (1994).
[50] M. Bauer, F. Baudenbacher, and H. Kinder, Physica C **246**, 113 (1995).
[51] Note that these threading dislocations must have a screw component in order to relieve the in-plane substrate-film misfit.
[52] V. Svetchnikov, V. Pan, C. Traeholt, and H. Zandbergen, IEEE Trans. Appl. Supercond. **7**, 1396 (1997).
[53] T. S. Ravi, D. M. Hwang, R. Ramesh, Siu Wai Chan, L. Nazar, C. Y. Chen, A. Inam, and T. Venkatesan, Phys. Rev. B **42**, 10 141 (1990).
[54] M. Kusunoki, Y. Takano, M. Makaida, and S. Ohshima, Physica C **321**, 81 (1999).
[55] S. K. Streiffer, B. M. Lairson, C. B. Eom, B. M. Clemens, J. C. Bravman, and T. H. Geballe, Phys. Rev. B **43**, 13 007 (1991).
[56] T. Haage, J. Zegenhagen, H.-U. Habermeier, and M. Cardona, Phys. Rev. Lett. **80**, 4225 (1998).
[57] J. G. Wen, T. Morishita, N. Koshizuka, C. Traeholt, and H. W. Zandbergen, Appl. Phys. Lett. **66**, 1830 (1995).
[58] H. W. Zandbergen, J. G. Wen, C. Traeholt, and V. Svetchnikov, J. Alloys Compd. **195**, 85 (1993).
[59] V. C. Matijasevic, B. Ilge, B. Stäuble-Pümpin, G. Rietveld, F. Tuinstra, and J. E. Mooij, Phys. Rev. Lett. **76**, 4765 (1996).
[60] J. A. Alarco, G. Brorsson, H. Olin, and E. Olsson, J. Appl. Phys. **75**, 3202 (1994).